ACS APPLIED MATERIALS & INTERFACES

Research Article

www.acsami.org

Three-Dimensional Macroporous Graphene–Li_2FeSiO_4 Composite as Cathode Material for Lithium-Ion Batteries with Superior Electrochemical Performances

Hai Zhu, Xiaozhen Wu, Ling Zan, and Youxiang Zhang*

College of Chemistry and Molecular Sciences, Wuhan University, Wuhan 430072, People's Republic of China

Supporting Information

ABSTRACT: Three-dimensional macroporous graphene-based Li_2FeSiO_4 composites (3D-G/Li_2FeSiO_4/C) were synthesized and tested as the cathode materials for lithium-ion batteries. To demonstrate the superiority of this structure, the composite's performances were compared with the performances of two-dimensional graphene nanosheets-based Li_2FeSiO_4 composites (2D-G/Li_2FeSiO_4/C) and Li_2FeSiO_4 composites without graphene (Li_2FeSiO_4/C). Due to the existence of electronic conductive graphene, both 3D-G/Li_2FeSiO_4/C and 2D-G/Li_2FeSiO_4/C showed much improved electrochemical performances than the Li_2FeSiO_4/C composite. When compared with the 2D-G/Li_2FeSiO_4/C composite, 3D-G/Li_2FeSiO_4/C exhibited even better performances, with the discharge capacities reaching 313, 255, 215, 180, 150, and 108 mAh g^{-1} at the charge–discharge rates of 0.1 C, 1 C, 2 C, 5 C, 10 C and 20 C (1 C = 166 mA g^{-1}), respectively. The 3D-G/Li_2FeSiO_4/C composite also showed excellent cyclability, with capacity retention exceeding 90% after cycling for 100 times at the charge–discharge rate of 1 C. The superior electrochemical properties of the 3D-G/Li_2FeSiO_4/C composite are attributed to its unique structure. Compared with 2D graphene nanosheets, which tend to assemble into macroscopic paper-like structures, 3D macroporous graphene can not only provide higher accessible surface area for the Li_2FeSiO_4 nanoparticles in the composite but also allow the electrolyte ions to diffuse inside and through the 3D network of the cathode material. Specially, the fabrication method described in this study is general and thus should be readily applicable to the other energy storage and conversion applications in which efficient ionic and electronic transport is critical.

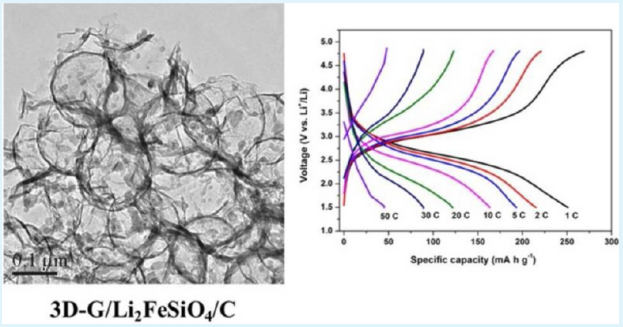

KEYWORDS: *Li_2FeSiO_4/C, macroporous, graphene, cathode materials, lithium-ion batteries*

INTRODUCTION

Rechargeable lithium-ion batteries are now in great demand to power portable electronic devices, store electricity from renewable energy sources, and as a vital component in electric vehicles.[1−3] For electrode materials in lithium-ion batteries, the main challenges are to achieve high capacities, excellent cycling performances and high rate capabilities. Lithium iron orthosilicate (Li_2FeSiO_4) has been considered as a promising cathode material because of its high theoretical capacity (theoretical capacity of the material rises to 332 mAh g^{-1} because the Fe^{4+}/Fe^{3+} redox reaction has been considered as possible.[4−6]), low cost, high thermal stability through strong Si–O bonding, increased safety and environmental friendliness. Unfortunately, the Li_2FeSiO_4 cathode materials reported so far have generally shown low rate capabilities resulting from the low electronic and ionic conductivities of the material (the specific electronic conductivity of Li_2FeSiO_4 was measured to be about 6×10^{-14} S cm^{-1} at room temperature[7]). Accordingly, much effort, including cation-doping,[8] nanoarchitecturing[9] and carbon coating,[10] has been made to improve the electrical properties of Li_2FeSiO_4. Of these methods, carbon coating is the most effective and facile.

Owing to its large surface area, excellent mechanical flexibility, superior electrical conductivity and high chemical and thermal stability, graphene has been utilized in the past few years in preparing various hybrid electrode materials for lithium-ion batteries.[11,12] For anodes, graphene can be introduced to absorb the volume changes and thus to improve the structure stability of the metal and metal oxides during the charge/discharge processes.[13,14] For cathodes, graphene is also beneficial because it facilitates the electron transport and Li^+ diffusion of the anchored materials, and thus enhances their electrochemical performances.[15] However, in most cases, two-dimensional (2D) graphene nanosheets were used in these hybrid electrode materials. The 2D graphene nanosheets, although having a lot of appealing properties, tend to assemble into macroscopic paper-like structures in a way that reduces the large accessible surface area of the material. This usually results from the irreversible agglomeration and restacking of the individual graphene nanosheets caused by the strong $\pi-\pi$ interactions

Received: April 24, 2014
Accepted: June 25, 2014
Published: June 25, 2014

and van der Waals force between the planar basal planes of the graphene nanosheets.

Recently, three-dimensional (3D) graphene architectures have been prepared in various ways, such as by self-assembly,[16,17] templated-assembly[18,19] and chemical vapor deposition (CVD) with 3D Ni foams as templates,[20,21] and have been used as the robust matrix for accommodating different transition metal oxides (MO) as electrode materials for supercapacitors.[18−24] This unique hierarchical architecture not only prevents serious restacking of graphene sheets but also allows electrolytes to freely diffuse inside and through the 3D graphene network. With large accessible specific surface area, interconnected conductive network and cross-linked macroporous structure, these 3D graphene network-based electrode materials exhibit much improved performances with respect to the 2D graphene sheets-based electrode materials for the supercapacitors.

Herein, we report the synthesis of 3D macroporous graphene−Li_2FeSiO_4 nanocomposites (3D-G/Li_2FeSiO_4/C) and their application as the cathode material for lithium-ion batteries. 2D graphene nanosheets−Li_2FeSiO_4 nanocomposites (2D-G/Li_2FeSiO_4/C) were also synthesized and their electrochemical properties were measured and compared with the 3D-G/Li_2FeSiO_4/C nanocomposites. Under the synergistic effects of 3D porous graphene framework and nanoscale carbon-coated Li_2FeSiO_4 particles, the 3D-G/Li_2FeSiO_4/C nanocomposite showed superior electrochemical performances as the cathode materials for lithium-ion batteries, with the specific discharge capacities reaching 315 and 120 mAh g^{-1} at the rate of 0.1 and 20 C (1 C = 166 mA g^{-1}), respectively.

EXPERIMENTAL SECTION

Synthesis of 3D Macroporous Graphene Framework. The 3D porous graphene framework was fabricated by a templated-assembly method. The first step of the synthesis was the preparation of graphene oxide (GO) dispersion in deionized water and (3-aminopropyl)-triethoxysilane (APTES)-modified silica (A-SiO_2) nanospheres. GO was obtained by ultrasonic treatment of graphite oxide, which was prepared using the traditional Hummers's method,[25] and then dispersed in deionized water with a concentration of 2 mg mL^{-1}. A-SiO_2 nanospheres were prepared according to the classical Stöber method.[26] Typically, $NH_3{\cdot}H_2O$ (6.5 mL) and TEOS (7 mL) were dissolved in aqueous ethanol solution. After 3.5 h, 0.28 mL of APTES was dropped into the solution and stirred for 24 h at room temperature to obtain APTES-modified silica nanospheres. A-SiO_2 nanospheres were harvested by centrifugation and washing with deionized water and ethanol. The A-SiO_2 nanospheres were redispersed in deionized water to obtain an aqueous suspension with a concentration of 2 mg mL^{-1} for later usage. The second step of the synthesis was to obtain GO nanosheets-encapsulated A-SiO_2 nanospheres via the electrostatic interaction between positively charged A-SiO_2 spheres and negatively charged GO sheets in aqueous solutions. In a typical process, the GO (70 mL) and A-SiO_2 (170 mL) dispersions were mixed at pH = 2. At this pH value, the GO nanosheets and the A-SiO_2 nanospheres were oppositely charged (GO, negative; A-SiO_2, positive) and thus electrostatic interactions existed between the two components, leading to the uniform distribution of A-SiO_2 nanospheres inside the GO sheets.[18] The GO encapsulated-A-SiO_2 nanoparticles precipitation was then vacuum-filtrated on a Millipore filter to realize the sandwich type assembly of A-SiO_2 spheres and GO sheets. The above composite film was peeled off from the filter, air-dried at 80 °C for overnight. The third step of the synthesis was to anneal the GO nanosheets-encapsulated A-SiO_2 nanospheres assembly at 800 °C for 30 min in a tubular furnace. In this annealing process, the GO in the assembly was thermally reduced into graphene with the 3D framework structure of the assembly fixed. The final macroporous networks were obtained by removing the silica nanospheres with 10% HF.

Synthesis of 2D Graphene Nanosheets. The 2D graphene nanosheets were synthesized by chemically reducing the GO nanosheets with hydrazine solution.[27] Hydrazine-reduced 2D graphene nanosheets were obtained by adding 100 mL of a 50% hydrazine solution into 100 mL of 0.5 mg mL^{-1} GO solution. The reaction process was carried out at 50 °C for 12 h. The final films were collected via filtration, washed with pure water several times and then dried at 90 °C.

Synthesis of 3D Macroporous Graphene-Li_2FeSiO_4 (3D-G/Li_2FeSiO_4/C) Nanocomposite. Typically, 65 mg of 3D macroporous graphene was dispersed in 50 mL of alcohol via strong ultrasonic agitation for 30 min. Next, 1 g of poly(ethylene glycol)-*block*-poly-(propylene glycol)-*block*-poly(ethylene glycol) P123 ($EO_{20}PO_{70}EO_{20}$) was dissolved in the above absolute alcohol under vigorous magnetic stirring. Then 4 mmol portion of lithium acetate, 2 mmol portion of ferric nitrate and 2 mmol of tetraethyl orthosilicate (TEOS, CP) were added into above solution in sequence and the mixture was stirred for 2 h. After that, the solution was heated at 70 °C and stirred simultaneously until the alcohol was completely evaporated. Finally, the xerogel was thoroughly grinded and annealed in a furnace tube filled with argon atmosphere at 600 °C for 10 h. When cooled to room temperature, the 3D-G/Li_2FeSiO_4/C composite was obtained.

Synthesis of 2D Graphene Nanosheets−Li_2FeSiO_4 (2D-G/Li_2FeSiO_4/C) Nanocomposite. The synthesis procedure of the 2D-G/Li_2FeSiO_4/C composite was the same as the synthesis procedure of 3D-G/Li_2FeSiO_4/C composite except that 2D graphene nanosheets, instead of 3D macroporous graphene frameworks, were used in the synthesis.

Synthesis of Li_2FeSiO_4/C Nanocomposite without Graphene. The synthesis procedure of the Li_2FeSiO_4/C composite was the same as the procedures of the 3D-G/Li_2FeSiO_4/C and 2D-G/Li_2FeSiO_4/C composites except that no graphene was used in the synthesis. This modified sol−gel synthesis method was used before by us to obtain Li_2FeSiO_4/C nanoparticles.[6]

Characterization. The morphologies of the materials (3D-G/Li_2FeSiO_4/C, 2D-G/Li_2FeSiO_4/C and Li_2FeSiO_4/C) were investigated using a field-emission scanning electron microscope (SIRION, FEI, USA). Transmission electron microscopy (TEM) images were taken on a JEM 2010-FEF (JEOL Ltd., Japan) operating at 200 kV. The crystal structural characterization of the samples was carried out on a Bruker D8 Advance X-ray diffractometer with Cu Kα radiation (λ = 0.154 06 nm). The Raman spectra were obtained by using a RM-1000 Renishaw confocal Raman microspectroscope with 514.5 nm laser radiation at a laser power of 0.04 mW in the range of 500−3000 cm^{-1}. The carbon contents in composites were determined with a VarioEL III elemental analyzer (Elementar Analysen System GmbH, Germany). For composite Li_2FeSiO_4/C without graphene, the carbon content is 18.3%. For the composites of 3D-G/Li_2FeSiO_4/C and 2D-G/Li_2FeSiO_4/C, the carbon contents are 23.5% and 23.8%, respectively. The Li:Fe ratios in the composites were determined by inductively coupled plasma atomic emission spectroscopy (ICP-AES). The ICP-AES elemental analysis showed that the Li:Fe ratios in the 3D-G/Li_2FeSiO_4/C, 2D-G/Li_2FeSiO_4/C and Li_2FeSiO_4/C composites are 2.00(2), 1.99(7) and 2.00(7), respectively.

Evaluation of Electrochemical Performances. The electrochemical measurements were carried out using CR2016 coin cells with lithium metal disks as the counter electrodes. The working electrodes were made by pressing mixtures of the active materials, acetylene black (AB) and polyvinylidene fluoride (PVDF) binder on stainless steel meshes that were used as the current collectors. For composites 3D-G/Li_2FeSiO_4/C and 2D-G/Li_2FeSiO_4/C with graphene, the composition of the cathode was composite:AB:PVDF = 75:20:5. For composite Li_2FeSiO_4/C without graphene, the composition of the cathode was adjusted to Li_2FeSiO_4/C:AB:PVDF = 70:25:5. With this adjustment, the total carbon contents in the cathodes are the same for all three composites (3D-G/Li_2FeSiO_4/C, 2D-G/Li_2FeSiO_4/C and Li_2FeSiO_4/C). The weight of active materials varied between 3.0 and 4.0 mg cm^{-2} for each cell. The electrolyte was composed with 1 M $LiPF_6$ in ethylene carbonate/dimethyl carbonate (1:1 v/v) solvents and the separator was Celgard 2300 microporous film. The cells were assembled in a glovebox filled with high purity Ar gas. The electrochemical tests were performed

Scheme 1. Illustrations of the Synthesis Procedures for the 3D Macroporous Graphene Framework (a) and for the 3D-G/Li_2FeSiO_4/C Composite (b)

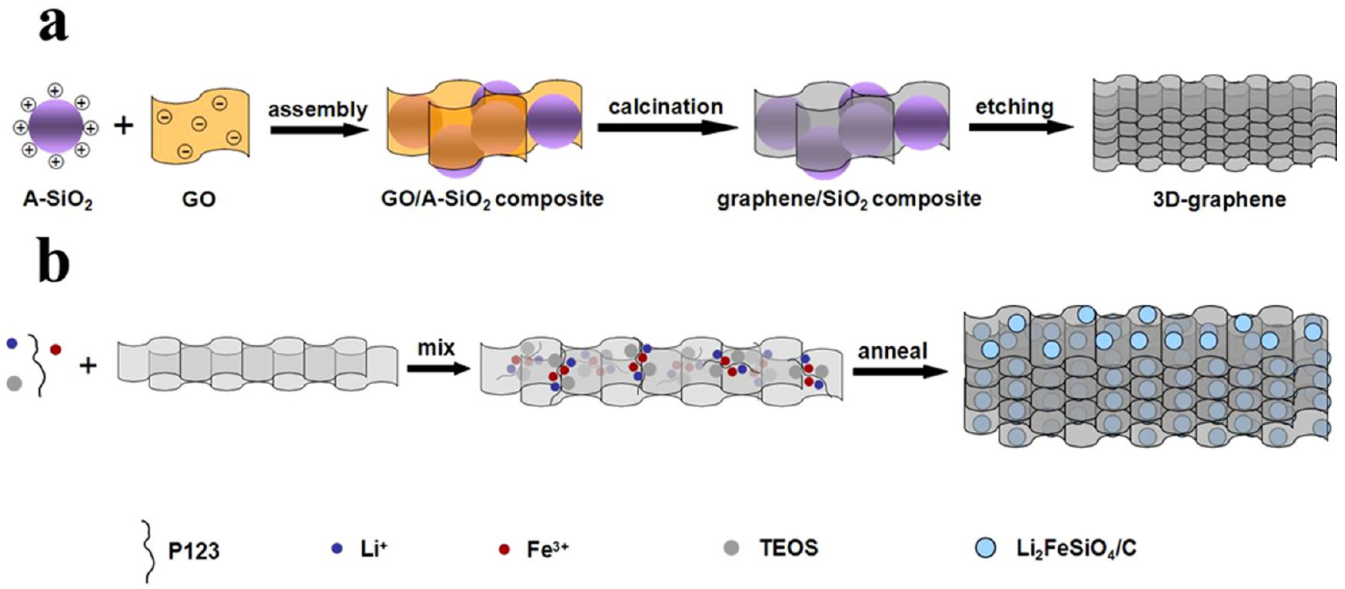

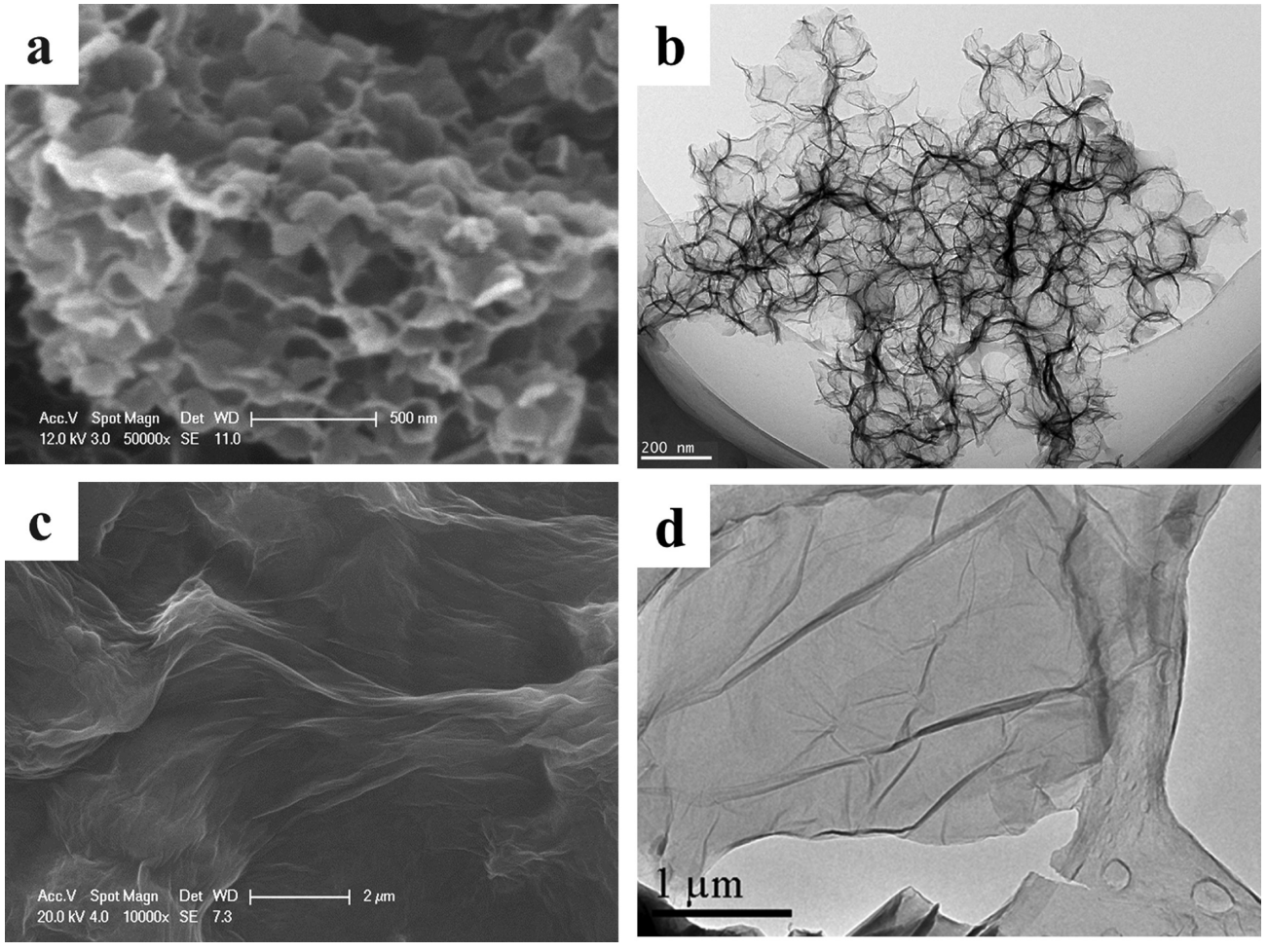

Figure 1. Morphology of the 3D graphene framework (a, b) and the 2D graphene nanosheets (c, d). The SEM image (a) and TEM image (b) of the 3D graphene framework show the interconnected macroporous character; the SEM image (c) and TEM image (d) of the 2D graphene nanosheets show the flexible planar features.

galvanostatically at different current densities with voltage window of 1.5−4.8 V on Neware battery test system (Shenzhen, China) at room temperature (20 °C). All the charge/discharge specific capacities were calculated on the net mass of Li_2FeSiO_4 excluding carbon content.

dx.doi.org/10.1021/am502408m | *ACS Appl. Mater. Interfaces* 2014, 6, 11724−11733

Electrochemical impedance spectroscopy (EIS) was conducted using a CHI760C electrochemistry workstation. The AC amplitude was 5 mV, and the frequency range applied was 100 kHz to 0.01 Hz. All the EIS were measured after the batteries were discharged to have a discharge capacity of 166 mA h g^{-1}.

RESULTS AND DISCUSSION

As shown in Scheme 1a, the 3D macroporous graphene framework was fabricated through a templated-assembly method. First, the surface grafted and positively charged SiO_2 spheres were assembled with negatively charged graphene oxide (GO) nanosheets by electrostatic interactions. After the assembled GO/SiO_2 composite was vacuum filtered and dried, it was calcinated at 800 °C to reduce the GO in the composite into graphene and fix the 3D framework structure. Finally, the SiO_2 spheres in the graphene/SiO_2 composite were removed using HF acid, leaving behind the 3D porous graphene framework. The synthesis procedure for the 3D-G/Li_2FeSiO_4/C composite is illustrated in Scheme 1b. After the 3D porous graphene framework was dispersed in ethanol, P123 and the precursors of Li_2FeSiO_4 were dissolved in the solution, forming a mixed suspension. After the ethanol in the above solution was evaporated at 70 °C, a gel was obtained. The gel was then dried and annealed at 600 °C in an Ar atmosphere to obtain the 3D-G/Li_2FeSiO_4/C composite. For comparison, graphene nanosheets (2D graphene) and the 2D-G/Li_2FeSiO_4/C composite were also synthesized. The 2D graphene was synthesized by hydrazine reduction of GO in solution, whereas the 2D-G/Li_2FeSiO_4/C composite was synthesized through the same procedures with the 3D-G/Li_2FeSiO_4/C composite except that 2D graphene nanosheets, instead of 3D macroporous graphene frameworks, were used in the process.

The XRD and Raman spectra of the 3D porous graphene frameworks and 2D graphene nanosheets are shown in Figures S1 and S2 in the Supporting Information. In the XRD spectra (Figure S1, Supporting Information), a broad characteristic diffraction peak can be observed at 26.6°, which corresponds to the (002) reflection of graphene sheets. In the Raman spectrum (Figure S2, Supporting Information) of 3D macroporous graphene, four prominent features can be observed. The G band, appearing at 1582 cm^{-1}, is a doubly degenerate phonon mode that is Raman active for the sp^2 carbon network. The D band, appearing at ~1350 cm^{-1}, is a defect-induced Raman feature,[28] which cannot be seen for single- and few-layer graphenes without any defects. Generally, the integrated intensity ratio I_D/I_G for the D band and G band can be used for characterizing the defect quantity in graphitic materials.[29] The appearance of the D band in this Raman spectrum can be understood because these graphenes were obtained by chemical methods, instead of through physical or micromechanical methods. For these multiple-layer graphenes with disorders and defects, the G′ band at ~2700 cm^{-1} is broad and weak. The Raman feature at ~2950 cm^{-1} is associated with a D + G combination mode and is also induced by disorders. The Raman spectrum of the 2D graphene nanosheets is very similar to that of the 3D graphene. The difference between these two spectra is that although the ratio of the D and G band intensities (I_D/I_G) is 0.66 for the 3D microporous graphenes, it is 0.70 for the 2D graphenes nanosheets.

Typical scanning electron microscopy (SEM) and TEM images of 3D porous graphene frameworks and 2D graphene nanosheets are shown in Figure 1. In the SEM image of the 3D graphene (Figure 1a), the open porous structures are obvious. The porous structure did not collapse after removing the SiO_2 template due to the interconnected nature of the multilayered graphene walls in the assembled 3D structure. From the TEM image (Figure 1b), we can further confirm that hollow macroporous bubbles are the basic building blocks of the 3D graphene frameworks. The pore sizes are measured to be about 150 nm. From the SEM image of 2D graphene nanosheets (Figure 1c), we can see that micrometer scale graphene sheets, although being very thin, are easy to be crumpled and agglomerated. The TEM image of the 2D graphene nanosheets (Figure 1d) also showed that the nanosheets can easily be wrinkled.

The porous feature and specific surface areas of the 3D graphene frameworks and 2D graphene nanosheets were analyzed by nitrogen adsorption−desorption measurements. The adsorption−desorption curve of the 3D graphene frameworks (Figure 2a) exhibits the typical characteristic of type-IV

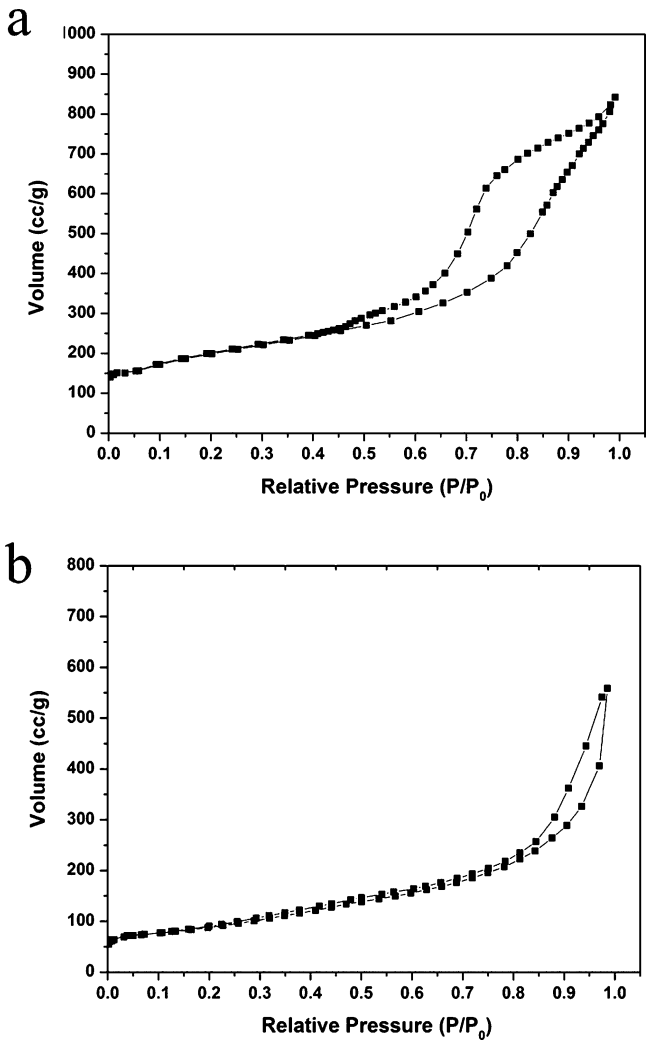

Figure 2. N_2 adsorption−desorption curves of the 3D macroporous graphene framework (a) and the 2D graphene nanosheets (b).

isotherms with a distinct hysteresis loop in the P/P_0 range of 0.4−1.0, indicating the presence of relatively large macropores in the frameworks. The N_2 adsorption−desorption curve of the 2D graphene nanosheets (Figure 2b) also shows a type-IV isotherm curve, but with a much less distinctive hysteresis loop in the P/P_0 range of 0.8−1.0. Although the Brunauer−Emmett−Teller (BET) analysis reveals a specific surface area of 883 m^2 g^{-1} and pore volume of 1.253 cm^3 g^{-1} for the 3D porous graphene

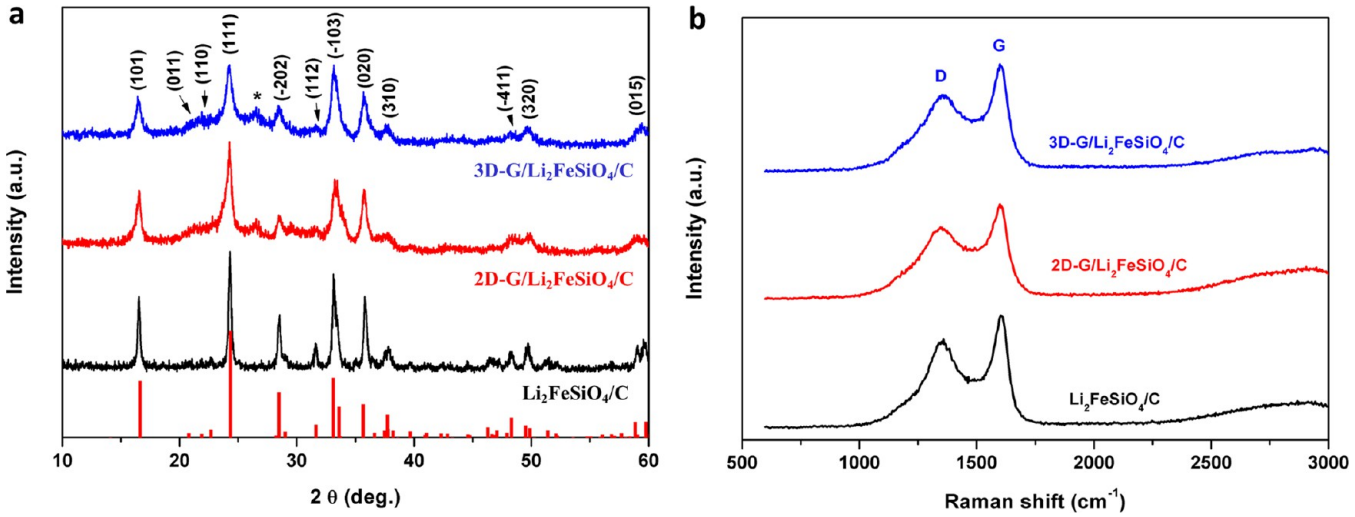

Figure 3. XRD patterns (a) and the Raman spectroscopies (b) of the composites.

frameworks, the specific surface area and pore volume are measured to be 463 $m^2\ g^{-1}$ and 0.159 $cm^3\ g^{-1}$, respectively, for the 2D graphene nanosheets.

The 3D-G/Li_2FeSiO_4/C, 2D-G/Li_2FeSiO_4/C and Li_2FeSiO_4/C composites were synthesized by a modified sol−gel method.[6] The X-ray diffraction (XRD) patterns and the Raman spectroscopes of these composites are measured and shown in Figure 3. In the XRD pattern of the Li_2FeSiO_4/C composite (Figure 3a), all the reflection peaks can be well indexed on the basis of the monoclinic structure reported by Nishimura et al.[30] (S.G. $P2_1/n$, a = 8.228 98 Å, b = 5.020 02 Å, c = 8.233 35 Å, and β = 99.2027°) without any peak from impurity phases. The 3D-G/Li_2FeSiO_4/C and 2D-G/Li_2FeSiO_4/C composites show the same XRD patterns as the pattern of Li_2FeSiO_4/C, except that the characteristic peak of graphene at 26.6° appears. Another obvious difference between the XRD patterns of the composites with and without graphene is that the reflection peaks of the composites with graphenes are broader and weaker than those of the composite without graphene. This difference indicates that, due to the existence of graphenes, the Li_2FeSiO_4 crystals in the 3D-G/Li_2FeSiO_4/C and 2D-G/Li_2FeSiO_4/C composites are smaller than the crystals in the Li_2FeSiO_4/C composite. Through Sherrer equation calculation ($B(2\theta) = 0.9\lambda/L_m\cos\ \theta$, where $B(2\theta)$ is the width of the (111) Bragg peak at half of its maximum intensity and L_m is the average crystal size), we can estimate that the average crystallite sizes are ~40, ~20 and ~18 nm for the Li_2FeSiO_4 crystals in the Li_2FeSiO_4/C, 2D-G/Li_2FeSiO_4/C and 3D-G/Li_2FeSiO_4/C composites, respectively. In the Raman spectroscopies (Figure 3b), all the composites show the same patterns and these patterns are very similar to the Raman patterns of the graphenes (Figure S2, Supporting Information). In the Raman spectrum of the Li_2FeSiO_4/C composite without graphene, the G band at 1582 cm^{-1} appears. Because the G band denotes the presence of the sp^2 carbon network, this result indicates that because large molecular weight polymer was used as the carbon source during the synthesis, part of the carbon in the composite is graphitized. Compared with the G′ band in the Raman spectra of the graphenes, due to the increase of disordered carbon in the composites, the intensities of the G′ band in the Raman spectra of the 3D-G/Li_2FeSiO_4/C and 2D-G/Li_2FeSiO_4/C composites decreased. The peak intensity ratio between the D and G bands (I_D/I_G) was used to evaluate the ratio between the sp^2 carbon network and sp^3 amorphous carbon in the composite (with a smaller ratio of I_D/I_G corresponding to a higher degree of graphitization). The I_D/I_G values of the Li_2FeSiO_4/C, 2D-G/Li_2FeSiO_4/C and 3D-G/Li_2FeSiO_4/C are 0.79, 0.77 and 0.73, respectively.

The SEM and TEM images of the 3D-G/Li_2FeSiO_4/C and 2D-G/Li_2FeSiO_4/C composites are shown in Figure 4. When no graphene was added into the precursor solution, the reaction products synthesized by this modified sol−gel method were Li_2FeSiO_4 nanoparticles coated by amorphous carbon (Li_2FeSiO_4/C) [ref 6]. The images of the 3D-G/Li_2FeSiO_4/C and 2D-G/Li_2FeSiO_4/C composites show that the 3D porous graphene frameworks and 2D graphene nanosheets presented in the precursor solution did not change the morphologies of the synthesis products. From the SEM image of 3D-G/Li_2FeSiO_4/C (Figure 4a), we can see that the macropores were still wide open, which will be useful for the electrolyte in the lithium-ion batteries to enter into the cathode. The TEM image of 3D-G/Li_2FeSiO_4/C (Figure 4b) revealed that Li_2FeSiO_4/C nanoparticles, with sizes in the range of 15−20 nm, were anchored to both the inside and outside of the microscale pores in the graphene matrix. Although the SEM image suggests that the nanoparticles on the surface of 3D graphene can aggregate together to form secondary particles, the TEM image shows that the nanoparticles inside the pores of the 3D frameworks are separately anchored on the graphene sheets, with their surfaces apt to be fully contacted with the electrolyte in the batteries. The HRTEM image (Figure 4c) confirms that Li_2FeSiO_4/C particles (~15 nm) are anchored to the 3D graphene matrix. From the HRTEM image (Figure 4d), the distance between the crystal lattice fringes is measured to be 0.312 nm (the top inset in Figure 4d), corresponding to the (−202) planes of monoclinic phase of Li_2FeSiO_4. This distance between the crystal planes of the Li_2FeSiO_4 nanoparticle, with the same value of 0.312 nm, can also be calculated according to the selected area electron diffraction (SAED) spots (the lower inset in Figure 4d). In comparison, in the SEM image of the 2D-G/Li_2FeSiO_4/C composite (Figure 4e), although most Li_2FeSiO_4/C nanoparticles are homogeneously anchored on the graphene nanosheets, there are still some nanoparticles aggregated together, and it is easy for the graphene nanosheets to be attached to each other and form thick paper-like structures. In the TEM image of the 2D-G/Li_2FeSiO_4/C composite (Figure 4f), we can see that although Li_2FeSiO_4 nanoparticles are anchored to the graphene matrix, the nanoparticles are not

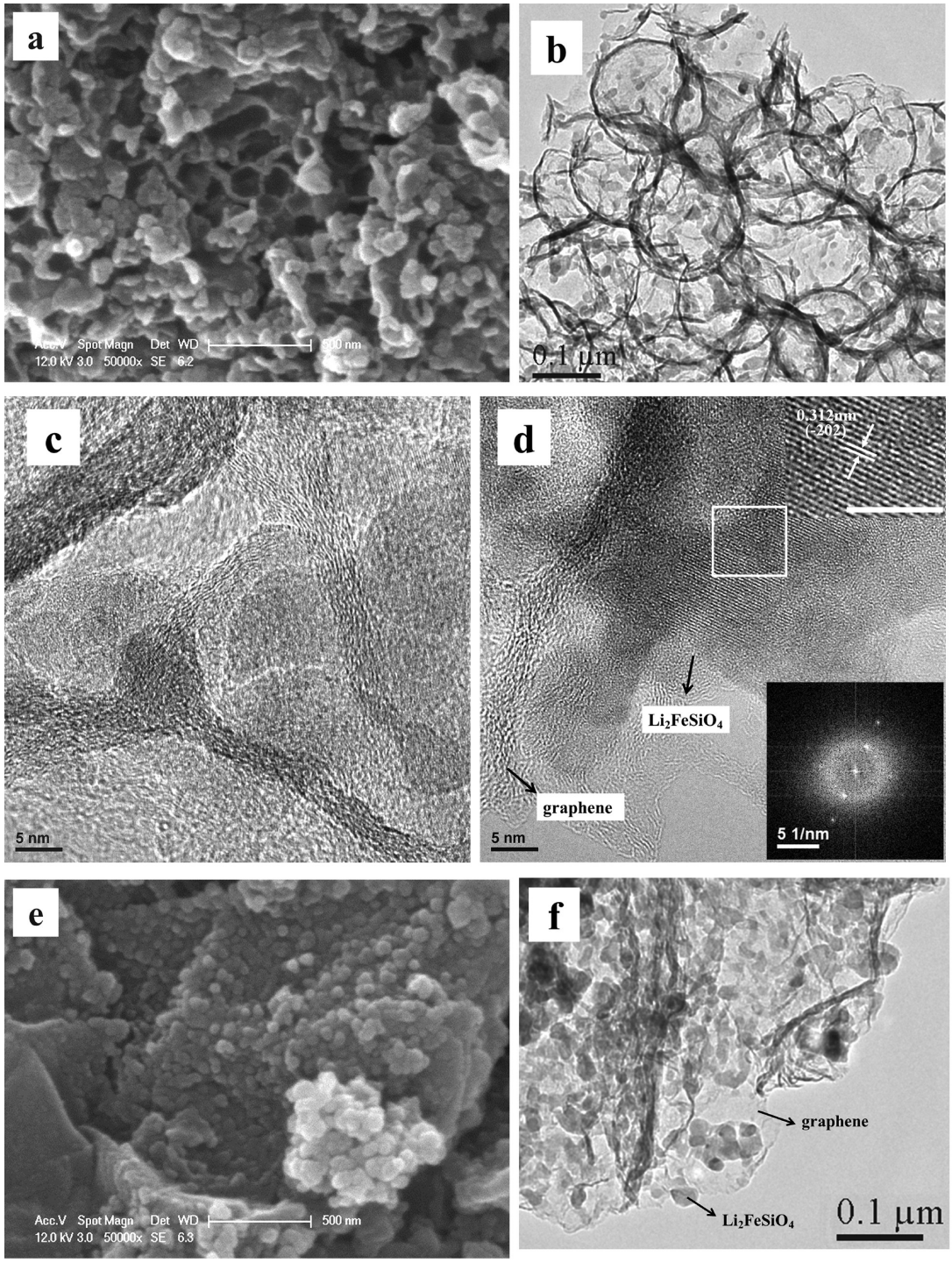

Figure 4. Morphologies and microstructures of the 3D-G/Li_2FeSiO_4/C and 2D-G/Li_2FeSiO_4/C composites. The SEM image (a) and TEM images (b, c, d) of 3D-G/Li_2FeSiO_4/C show that the nanoscale Li_2FeSiO_4/C particles are anchored on the 3D graphene framework uniformly, with nanoparticles both inside and outside of the macropores. The SEM image (e) and TEM image (f) of 2D-G/Li_2FeSiO_4/C show that the nanoparticles are dispersed closely on the wrinkled graphene nanosheets.

dispersed uniformly like those of the 3D-G/Li_2FeSiO_4/C composite. By comparing the morphologies and microstructures of the three composites (Li_2FeSiO_4/C, 2D-G/Li_2FeSiO_4/C and 3D-G/Li_2FeSiO_4/C), it can be concluded that both 2D graphene nanosheets and 3D porous graphene frameworks can help to reduce the sizes of the nanoparticles, and that, compared with 2D graphene nanosheets, 3D porous graphene frameworks can restrict the aggregation of the nanoscale particles.

When assembled into rechargeable lithium-ion batteries as the cathode materials, both 3D-G/Li_2FeSiO_4/C and 2D-G/Li_2FeSiO_4/C showed excellent electrochemical performances. Galvanostatic charge−discharge measurements were carried out with lithium metals as the anodes at a current density of 0.1 C (1 C = 166 mA g^{-1}) to evaluate the electrochemical properties of the 3D-G/Li_2FeSiO_4/C and 2D-G/Li_2FeSiO_4/C composites. Both composites showed the same charge−discharge curves

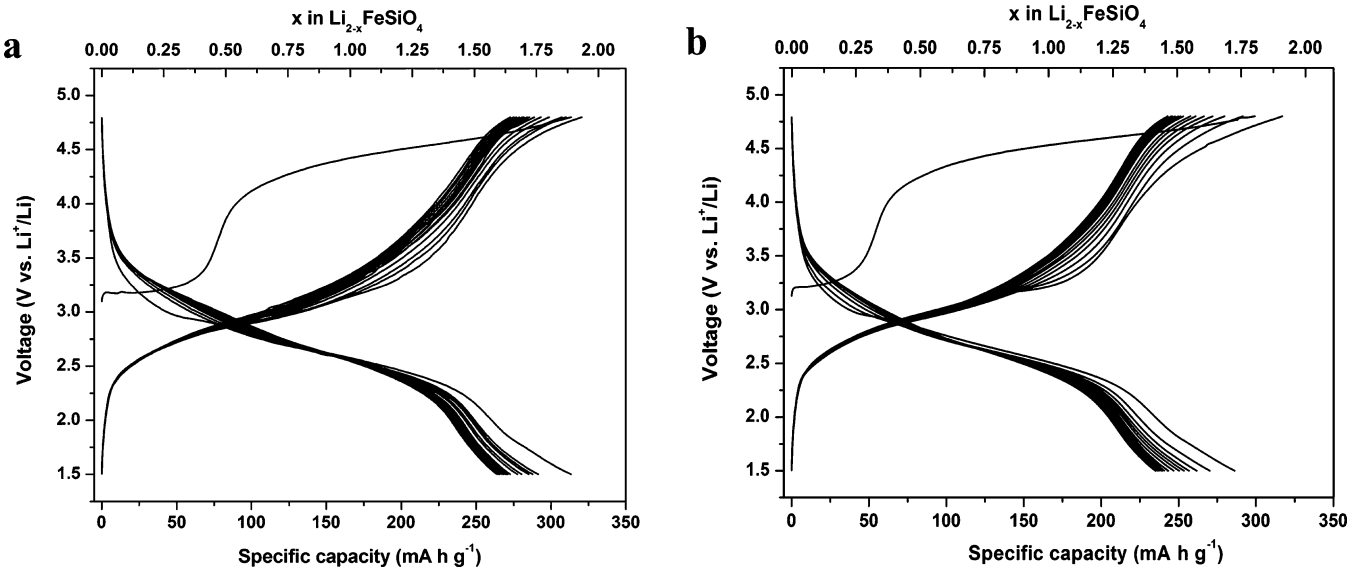

Figure 5. Voltage-specific capacity curves of the initial 15 cycles for the 3D-G/Li_2FeSiO_4/C (a) and 2D-G/Li_2FeSiO_4/C (b) composites recorded at 0.1 C and room temperature between 1.5 and 4.8 V (vs Li^+/Li).

(Figure 5) at 0.1 C between 1.5 and 4.8 V (vs Li^+/Li). The charge profile of the first cycle exhibits two voltage plateaus, located around 3.2 and ~4.3 V, respectively. The first voltage plateau (~3.2 V) corresponds to the Fe^{2+}/Fe^{3+} redox couple, as proved by Thomas et al.[31] The second voltage plateau (~4.3 V) should correspond to the Fe^{3+}/Fe^{4+} redox couple, as suggested by the ex situ Mössbauer spectroscopy measurements reported in recent literature.[4−6] In the discharge profile of the first cycle, a lowering of the potential plateaus can be observed, which was explained by a structural rearrangement involving the position-interchanging between the Li ions and Fe ions.[31] For the composite of 3D-G/Li_2FeSiO_4/C (Figure 5a), the discharge capacity in the first cycle is 313 mAh g^{-1}, which is 93% of the theoretical capacity of 332 mAh g^{-1} (corresponding to 2 Li^+ extraction/insertion per Li_2FeSiO_4 molecule). The discharge capacity in the 2nd cycle (291 mAh g^{-1}) shows a decay of 22 mAh g^{-1} from the capacity in the 1st cycle. The discharge capacity in the 15th cycle is 265 mAh g^{-1}, which is 91% of the discharge capacity in the 2nd cycle. For the composite of 2D-G/Li_2FeSiO_4/C (Figure 5b), although the electrochemical performances are also excellent, it still shows some inferiority when compared with the composite of 3D-G/Li_2FeSiO_4/C. The discharge capacities in the 1st, 2nd and 15th cycles are 286, 270 and 235 mAh g^{-1}, respectively, which are 91.4%, 92.8% and 88.6%, respectively, of the discharge capacities in the 1st, 2nd and 15th cycles for the composite of 3D-G/Li_2FeSiO_4/C. Capacity decay of these high-capacity composites at low current density (Figure S3, Supporting Information) indicates that side reactions with the cell electrolyte at high potentials are inevitable and detrimental to the cycling stability.

The electrochemical performances of the composites at high rates were also measured and are shown in Figure 6. Figure 6a shows the typical charge−discharge profiles of the 3D-G/Li_2FeSiO_4/C composite at various high rates. Discharge specific capacities of 255, 215, 180, 150, 120, 90 and 45 mAh g^{-1} can be reached at the rates of 1 C, 2 C, 5 C, 10 C, 20 C, 30 C and 50 C, respectively. As far as we know, these obtained capacities are very high for the Li_2FeSiO_4 material at room temperature when compared with the capacity values reported in literature.[4−10] At the same time, these discharge capacities prove again that more than one Li^+ per molecule can be extracted/inserted from/into Li_2FeSiO_4 (because the theoretical capacity is 166 mAh g^{-1} for 1 Li^+ transition per Li_2FeSiO_4 molecule) during the charge/discharge process. For example, at the rate of 1 C, the discharge capacity can be stabilized at 250 mAh g^{-1}, corresponding to 1.5 Li^+ ion per Li_2FeSiO_4 molecule. Even at a high rate of 5 C, the 3D-G/Li_2FeSiO_4/C composite, with a discharge capacity around 180 mAh g^{-1}, still can deliver more than one Li^+ per molecule. Figure 6b shows the typical charge−discharge profiles of composite 2D-G/Li_2FeSiO_4/C at various high rates. At high rates of 1 C, 2 C, 5 C, 10 C, 20 C and 30 C, discharge capacities of 204, 190, 165, 135, 105 and 70 mAh g^{-1} can be obtained, respectively. Although these discharge capacities are high enough when compared with the capacities reported in literature, they are lower than the discharge capacities of composite 3D-G/Li_2FeSiO_4/C when they are charged−discharged at the same rates. For example, at the rate of 1 C, composite 2D-G/Li_2FeSiO_4/C showed a discharge capacity of 204 mAh g^{-1} whereas composite 3D-G/Li_2FeSiO_4/C showed a discharge capacity of 250 mAh g^{-1}. Figure 6c shows the typical charge−discharge profiles of composite Li_2FeSiO_4/C at different high rates. When we compare Figure 6c with Figure 6a and 6b, the effects of graphene, 3D porous frameworks or 2D nanosheets, are obvious, because discharge capacities of only 160, 130, 100 and 80 mAh g^{-1} can be obtained at rates of 1 C, 2 C, 5 C and 10 C, respectively, for a Li_2FeSiO_4/C composite without graphene.

The cycling performances of composite 3D-G/Li_2FeSiO_4/C at various high rates are shown in Figure 6d,e. It can be seen that 3D-G/Li_2FeSiO_4/C exhibits a stable cyclability at various high rates. Specially, Figure 6e shows that after charging−discharging for 1000 times, composite 3D-G/Li_2FeSiO_4/C still has discharge capacities of 108, 82 and 45 mAh g^{-1} at the high rates of 20, 30 and 50 C, respectively, demonstrating both the high capacities and stable cyclabilities of the composite. From Figure 6f, we can see that composite 2D-G/Li_2FeSiO_4/C, although exhibited much better performances than composite Li_2FeSiO_4/C, had lower specific discharge capacities than composite 3D-G/Li_2FeSiO_4/C at all the high charge−discharge rates as a result of insufficient usage of the graphene nanosheets.

To further identify the kinetic properties of the 3D-G/Li_2FeSiO_4/C, 2D-G/Li_2FeSiO_4/C and Li_2FeSiO_4/C nanocomposites, EIS

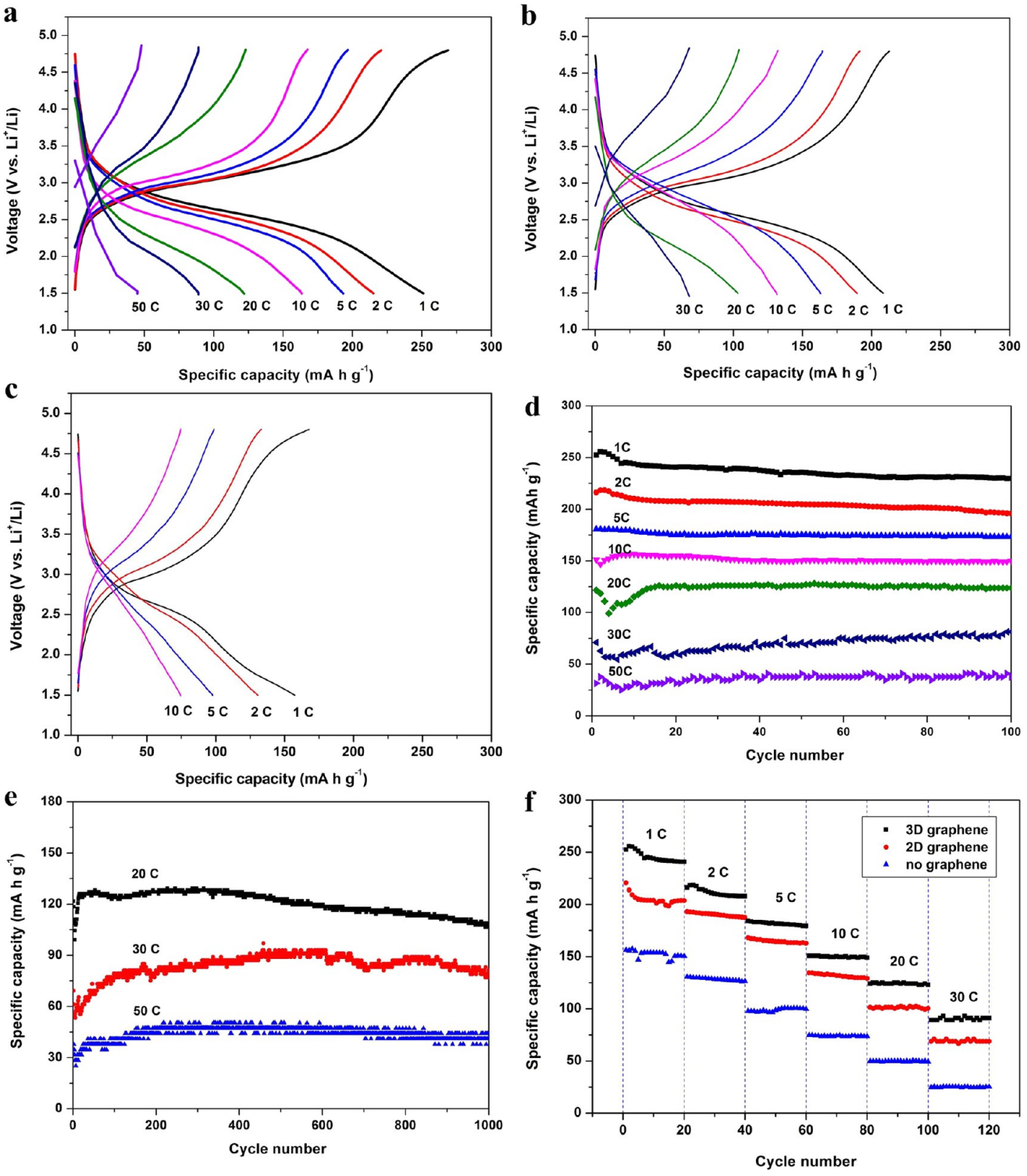

Figure 6. Electrochemical properties of the 3D-G/Li_2FeSiO_4/C, 2D-G/Li_2FeSiO_4/C and Li_2FeSiO_4/C composites as the cathode materials for lithium-ion batteries. Panels a, b and c show the typical charge−discharge curves at various high rates for 3D-G/Li_2FeSiO_4/C (a), 2D-G/Li_2FeSiO_4/C (b) and Li_2FeSiO_4/C (c). Panels d and e show the cyclability for the 3D-G/Li_2FeSiO_4/C composite. The comparison of the capabilities at various high rates for the three composites is shown in panel f.

measurements of the electrodes were conducted and are presented in Figure 7. All of EIS spectra are composed of a semicircle at the high to medium frequency region, which describes the charge transfer resistance (R_{ct}) for electrodes, and an inclined line in the low frequency range, which could be considered as Warburg impedance (Z_w) associated with the diffusion of the lithium ions into the bulk of the active material.[32] From comparing the diameters of the semicircles, we can see that the charge-transfer resistance for the 3D-G/Li_2FeSiO_4/C cathode is much smaller than the resistances for the 2D-G/Li_2FeSiO_4/C and Li_2FeSiO_4/C cathodes. The decreasing R_{ct} trend from the samples without graphene to the 3D porous graphene-based counterparts should be associated with the increasing conductivities of the cathode materials. For the 3D-G/Li_2FeSiO_4/C and 2D-G/Li_2FeSiO_4/C composites, with the

dx.doi.org/10.1021/am502408m | ACS Appl. Mater. Interfaces 2014, 6, 11724−11733

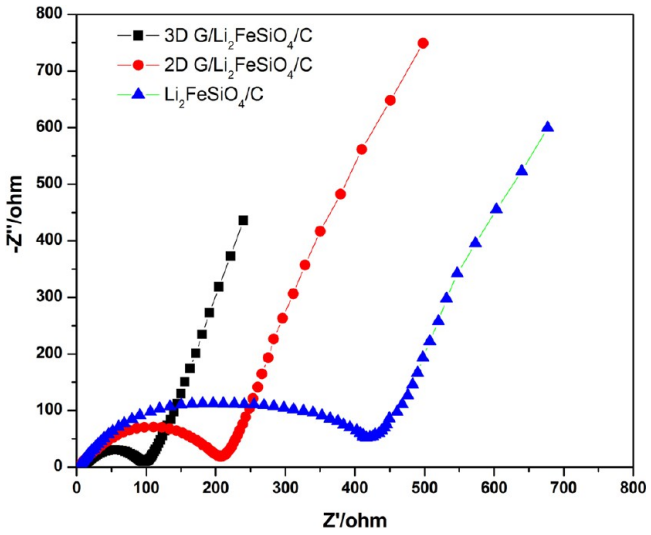

Figure 7. EIS measurements of the electrodes.

addition of electronic conductive graphenes into these extremely insulating silicates, the conductivities of the composites are much higher than the composites without graphene. Although both the graphenes are good electronic conductors (the conductivities were measured as 3.24×10^3 and 2.35×10^2 S m^{-1} for the 3D macroporous graphene and the 2D graphene nanosheets, respectively), the conductivity of the 3D graphene is more than 10 times higher than that of the 2D graphene. At the low frequency region, a more vertical straight line is shown for composite 3D-G/Li_2FeSiO_4/C than for composites 2D-G/Li_2FeSiO_4/C and Li_2FeSiO_4/C. This result implies that the lithium ions in electrolyte move more easily into 3D porous channels than moving into 2D packed structures.

The superior capabilities of composites 3D-G/Li_2FeSiO_4/C and 2D-G/Li_2FeSiO_4/C are believed to be the cooperative results of three factors. First, the nanoscale sizes of the Li_2FeSiO_4 particles guarantee short lithium diffusion path lengths, which are necessary for fast Li^+ extraction and insertion. Second, the good contact between the graphene nanosheets and the Li_2FeSiO_4/C nanoparticles ensure low contact resistance and tight adhesion between them, which are beneficial to the cyclabilities. Third, the conducting network formed by the graphene nanosheets in the composite serves as a fast three-dimensional path for electron migration during the charge−discharge processes. The better electrochemical performances of composite 3D-G/Li_2FeSiO_4/C than composite 2D-G/Li_2FeSiO_4/C should be attributed to our rationally designed 3D macroporous graphene architecture. In comparison with the 2D graphene with paper-like structures, the 3D graphene frameworks with macroporous features and high surface areas provide more efficient electrical and ionic transfer pathways. The high conductivity and high specific surface area of the 3D macroporous graphene frameworks serve as a double highway for electron transfer and electrolyte ions easy access to the electrode surfaces, which contribute to the much improved reversible capacities and rate capabilities.

CONCLUSIONS

In summary, we have synthesized 3D macroporous graphene framework-based Li_2FeSiO_4 nanocomposites and measured their electrochemical properties as the cathode materials for lithium-ion batteries. For comparison, 2D graphene nanosheets-based Li_2FeSiO_4 nanocomposites and Li_2FeSiO_4 nanocomposites without graphene have also been synthesized and measured as the cathode materials for lithium-ion batteries. Due to the existence of graphene and thus the much higher conductivities, both 3D macroporous graphene framework-based and 2D graphene nanosheets-based Li_2FeSiO_4 composites showed much higher capacities than the Li_2FeSiO_4 composite without graphene. Compared with 2D graphene nanosheets, which tend to assemble into macroscopic paper-like structures, 3D macroporous graphene frameworks can not only provide higher accessible surface area and higher electronic conductivity for the composites but also allow the electrolyte ions to freely diffuse inside and through the 3D network of the cathode. With large accessible specific surface area, interconnected conductive network and cross-linked macroporous structure, the 3D macroporous graphene framework-based Li_2FeSiO_4 exhibits improved performances with respect to the 2D graphene nanosheets-based Li_2FeSiO_4 materials. For 3D macroporous graphene framework-based Li_2FeSiO_4, very high discharge capacities of 313, 250, 215, 180, 150, 120, 90 and 45 mAh g^{-1} can be reached at the charge−discharge rates of 0.1 C, 1 C, 2 C, 5 C, 10 C, 20 C, 30 C and 50 C, respectively. For the cyclability, after charging−discharging for 1000 times at the rates of 30 C and 50 C, the composite still shows discharge capacities as high as 82 and 45 mAh g^{-1}, respectively.

ASSOCIATED CONTENT

Supporting Information

XRD spectra of the 3D porous graphene frameworks and 2D graphene nanosheets, Raman spectra of the 3D porous graphene frameworks and 2D graphene nanosheets, and the cyclabilities of the 3D-G/Li_2FeSiO_4/C and 2D-G/Li_2FeSiO_4/C composites at the rate of 0.1 C (16.6 mA g^{-1}). This material is available free of charge via the Internet at http://pubs.acs.org.

AUTHOR INFORMATION

Corresponding Author

*Y. Zhang. E-mail: yxzhang04@whu.edu.cn. Tel: +86-27-6578-3395. Fax: +86-27-6875-4067.

Notes

The authors declare no competing financial interest.

ACKNOWLEDGMENTS

The authors thank the Center for Electron Microscopy at Wuhan University for help in taking the TEM and high-resolution TEM images for the materials. This study was supported by the National Science Foundation of China (grants No. 20901062 and 21271145) and the China Scholarship Council (CSC, file No. 201208420526).

REFERENCES

(1) Tarascon, J. M.; Armand, M. Issues and Challenges Facing Rechargeable Lithium Batteries. *Nature* **2001**, *414*, 359−367.

(2) Armand, M.; Tarascon, J. M. Building Better Batteries. *Nature* **2008**, *451*, 652−657.

(3) Goodenough, J. B.; Kim, Y. Challenges for Rechargeable Li Batteries. *Chem. Mater.* **2010**, *22*, 587−603.

(4) Muraliganth, T.; Stroukoff, K. R.; Manthiram, A. Microwave-Solvothermal Synthesis of Nanostructured Li_2MSiO_4/C (M = Mn and Fe) Cathodes for Lithium-Ion Batteries. *Chem. Mater.* **2010**, *22*, 5754−5761.

(5) Lv, D. P.; Wen, W.; Huang, X. K.; Bai, J. Y.; Mi, J. X.; Wu, S. Q.; Yang, Y. A Novel Li_2FeSiO_4/C Composite: Synthesis, Characterization and High Storage Capacity. *J. Mater. Chem.* **2011**, *21*, 9506−9512.

(6) Wu, X. Z.; Jiang, X.; Huo, Q. S.; Zhang, Y. X. Facile Synthesis of Li_2FeSiO_4/C Composites with Triblock Copolymer P123 and Their

Application as Cathode Materials for Lithium Ion Batteries. *Electrochim. Acta* **2012**, *80*, 50−55.
(7) Dominko, R. Li_2MSiO_4 (M = Fe and/or Mn) Cathode Materials. *J. Power Sources* **2008**, *184*, 462−468.
(8) Dominko, R.; Sirisopanaporn, C.; Masquelier, C.; Hanzel, D.; Arcon, I.; Gaberscek, M. On the Origin of the Electrochemical Capacity of $Li_2Fe_{0.8}Mn_{0.2}SiO_4$. *J. Electrochem. Soc.* **2010**, *157*, A1309−A1316.
(9) Rangappa, D.; Murukanahally, K. D.; Tomai, T.; Unemoto, A.; Honma, I. Ultrathin Nanosheets of Li_2MSiO_4 (M = Fe, Mn) as High-Capacity Li-ion Battery Electrode. *Nano Lett.* **2012**, *12*, 1146−1151.
(10) Zheng, Z.; Wang, Y.; Zhang, A.; Zhang, T.; Cheng, F.; Tao, Z.; Chen, J. Porous Li_2FeSiO_4/C Nanocomposite as the Cathode Material of Lithium-Ion Batteries. *J. Power Sources* **2012**, *198*, 229−235.
(11) Han, S.; Wu, D. Q.; Li, S.; Zhang, F.; Feng, X. L. Graphene: A Two-Dimensional Platform for Lithium Storage. *Small* **2013**, *9*, 1173−1187.
(12) Kucinskis, G.; Bajars, G.; Kleperis, J. Graphene in Lithium Ion Battery Cathode Materials: A Review. *J. Power Sources* **2013**, *240*, 66−79.
(13) Yang, S. B.; Feng, X. L.; Ivanovici, S.; Müllen, K. Fabrication of Graphene-Encapsulated Oxide Nanoparticles: Towards High-Performance Anode Materials for Lithium Storage. *Angew. Chem., Int. Ed.* **2010**, *49*, 8408−8411.
(14) Zhou, G. M.; Wang, D. W.; Li, F.; Zhang, L.; Li, N.; Wu, Z. S.; Wen, L.; Lu, G. Q.; Cheng, H. M. Graphene-Wrapped Fe_3O_4 Anode Material with Improved Reversible Capacity and Cyclic Stability for Lithium Ion Batteries. *Chem. Mater.* **2010**, *22*, 5306−5313.
(15) Wang, H. L.; Yang, Y.; Liang, Y. Y.; Cui, L. F.; Casalongue, H. S.; Li, Y. G.; Hong, G. S.; Cui, Y.; Dai, H. J. $LiMn_{1-x}Fe_xPO_4$ Nanorods Grown on Graphene Sheets for Ultrahigh-Rate-Performance Lithium Ion Batteries. *Angew. Chem., Int. Ed.* **2011**, *50*, 7364−7368.
(16) Xu, Y. X.; Sheng, K. X.; Li, C.; Shi, G. Q. Self-Assembled Graphene Hydrogel via a One-Step Hydrothermal Process. *ACS Nano* **2010**, *4*, 4324−4330.
(17) Chen, W. F.; Yan, L. F. In Situ Self-assembly of Mild Chemical Reduction Graphene for Three-Dimensional Architectures. *Nanoscale* **2011**, *3*, 3132−3137.
(18) Choi, B. G.; Yang, M. H.; Hong, W. H.; Choi, J. W.; Huh, Y. S. 3D Macroporous Graphene Frameworks for Supercapacitors with High Energy and Power Densities. *ACS Nano* **2012**, *6*, 4020−4028.
(19) Chen, C. M.; Zhang, Q.; Huang, C. H.; Zhao, X. C.; Zhang, B. S.; Kong, Q. Q.; Wang, M. Z.; Yang, Y. G.; Cai, R.; Su, D. S. Macroporous "Bubble" Graphene Film via Template-Directed Ordered-Assembly for High Rate Supercapacitors. *Chem. Commun.* **2012**, *48*, 7149−7151.
(20) Cao, X. H.; Shi, Y. M.; Shi, W. H.; Lu, G.; Huang, X.; Yan, Q. Y.; Zhang, Q. C.; Zhang, H. Preparation of Novel 3D Graphene Networks for Supercapacitor Applications. *Small* **2011**, *7*, 3163−3168.
(21) He, Y. M.; Chen, W. J.; Li, X. D.; Zhang, Z. X.; Fu, J. C.; Zhao, C. H.; Xie, E. Q. Freestanding Three-Dimensional Graphene/MnO_2 Composite Networks As Ultra-light and Flexible Supercapacitor Electrode. *ACS Nano* **2013**, *7*, 174−182.
(22) Dong, X. C.; Xu, H.; Wang, X. W.; Huang, Y. X.; Chan-Park, M. B.; Zhang, H.; Wang, L. H.; Huang, W.; Chen, P. 3D Graphene-Cobalt Oxide Electrode for High-Performance Supercapacitor and Enzymeless Glucose Detection. *ACS Nano* **2012**, *6*, 3206−3213.
(23) Xu, Y. X.; Lin, Z. Y.; Huang, X. Q.; Liu, Y.; Huang, Y.; Duan, X. F. Flexible Solid-State Supercapacitors Based on Three-Dimensional Graphene Hydrogel Films. *ACS Nano* **2013**, *7*, 4042−4049.
(24) Wu, Z. S.; Sun, Y.; Tan, Y. Z.; Yang, S. B.; Feng, X.; Müllen, K. Three-Dimensional Graphene-Based Macro- and Mesoporous Frameworks for High-Performance Electrochemical Capacitive Energy Storage. *J. Am. Chem. Soc.* **2012**, *134*, 19532−19535.
(25) Hummers, W. S.; Offeman, R. E. Preparation of Graphene Oxide. *J. Am. Chem. Soc.* **1958**, *80*, 1339−1339.
(26) Stober, W.; Fink, A.; Bohn, E. Controlled Growth of Monodisperse Silica Spheres in Micron Size Range. *J. Colloid Interface Sci.* **1968**, *26*, 62−69.
(27) Zhou, Y.; Bao, Q.; Zhong, Y.; Loh, K. P. Hydrothermal Dehydration for the "Green" Reduction of Exfoliated Graphene Oxide to Graphene and Demonstration of Tunable Optical Limiting Properties. *Chem. Mater.* **2009**, *21*, 2950−2956.
(28) Pimenta, M. A.; Dresselhaus, G.; Dresselhaus, M. S.; Cancado, L. G.; Jorio, A.; Saito, R. Studying Disorder in Graphite-Based Systems by Raman Spectroscopy. *Phys. Chem. Chem. Phys.* **2007**, *9*, 1276−1291.
(29) Bonhomme, F.; Lassegues, J. C.; Servant, L. Raman Spectroelectrochemistry of a Carbon Supercapacitor. *J. Electrochem. Soc.* **2001**, *148*, E450−E458.
(30) Nishimura, S. I.; Hayase, S.; Kanno, R.; Yashima, M.; Nakayama, N.; Yamada, A. Structure of Li_2FeSiO_4. *J. Am. Chem. Soc.* **2008**, *130*, 13212−13213.
(31) Nyten, A.; Kamali, S.; Haggstrom, L.; Gustafsson, T.; Thomas, J. O. The Lithium Extraction/Insertion Mechanism in Li_2FeSiO_4. *J. Mater. Chem.* **2006**, *16*, 2266−2272.
(32) Murugan, A. V.; Muraliganth, T.; Manthiram, A. One-Pot Microwave-Hydrothermal Synthesis and Characterization of Carbon-Coated $LiMPO_4$ (M = Mn, Fe, and Co) Cathodes. *J. Electrochem. Soc.* **2009**, *156*, A79−A83.